Mapping of Local Corrosion Behavior of Zinc in Substitute Ocean Water at Its Initial Stages by SVET

E. Mena[1], L. Veleva[1,*], R. M. Souto[2,3]

[1] Department of Applied Physics, Research Center for Advanced Study (CINVESTAV-IPN), Mérida Carr. Ant. a Progreso Km. 6, 97310, Mérida, Yucatán, México
[2] Department of Chemistry, Universidad de La Laguna, P.O. Box 456, 38200 La Laguna, Tenerife, Canary Islands, Spain
[3] Institute of Material Science and Nanotechnology, Universidad de La Laguna, E-38200 La Laguna, Tenerife, Canary Islands, Spain
[*]E-mail: veleva@mda.cinvestav.mx

The recent advent of a number of local probe techniques is greatly contributing to overcome some limitations when applied to the investigation of corrosion processes *in situ*. The scanning vibrating electrode technique is one of them, and it is based upon the measurement of potential field distributions in the electrolyte surrounding an electrochemically-active surface. The localized distributions of anodic and cathodic activities on zinc metal/electrolyte interface, exposed to substitute ocean water (diluted 1:1000), have been mapped in situ using SVET. The data provide in situ information on the local ionic fluxes produced in the electrolyte as result of the electrochemical corrosion reactions that occurred on the zinc surface, even in the first hours of the process. The maps demonstrated the evolution of the corrosion process, since the nucleation and propagation of corroding pits on the metal. The time evolution of the maps allows to more adequately characterize the complex chemical process involved in zinc corrosion in sea-water with high spatial resolution.

1. INTRODUCTION

Zinc has a wide range of applications in corrosion protection, due to its low price and practical uses. For example, it is commonly used as sacrificial anode on ships' hulls. Furthermore, this metal is extensively employed in the production of hot dip galvanized steel, whose performance in sea water as

bridges, docks, tubes for water transport, among others marine structures, is an increasing topic of study.

Corrosion reactions occur due to the development of electrochemical microcells on a metal surface when in contact with an aqueous phase. In this way, Zn^{2+} ions are released from the anodic sites whereas OH^- ions are formed at the cathodic sites. In addition, these ionic species may interact giving origin to a variety of scarcely soluble zinc oxides/hydroxides that often precipitate on the surface of the exposed material [1,2]. In marine environments, retrieved zinc samples evidence that corrosion products exhibit more complex chemical structures due to the participation of anions present in sea water, such as chloride, carbonate and sulphate ions [3], which are usually revealed by X-ray diffraction. The application of conventional electrochemical techniques has shown that these precipitates act as an electrochemical barrier on the metal [4], though they exhibit voids when imaged using electron microscopies such as SEM and TEM [4]. Unfortunately, this knowledge is mostly based on the application of ex situ surface analytical techniques on retrieved samples, whereas in situ characterization using electrochemical methods only give average responses of the complete exposed surface. As result, the knowledge available on the corrosion of zinc in sea water corresponds to late stages of the corrosion process, when the precipitation of corrosion products on the surface has already produced protecting barrier layers, effectively modifying the corrosion mechanism. That is, they lack in situ information regarding the initiation of the corrosion process and its early propagation stages, when metal ions are released from the metal surface to the surrounding environment (i.e., zinc runoff).

These limitations for the in situ study of corroding systems can be overcome using spatially-resolved microelectrochemical techniques sensitive to the local differences in chemical reactivity that occur during the development of microcells on the metal surface [5-8], thus contributing to a better description of corrosion phenomena. Among these methods, the scanning electrochemical microscope (SECM) and the scanning vibrating electrode technique (SVET) have shown the greater applicability for the investigation of corrosion processes [8,9]. In the SECM, an electrochemical reaction occurring at the interface of a mobile ultra-microelectrode (UME) immersed in an electrolyte solution is employed for chemical imaging, because the magnitude of the faradaic current flowing through the tip depends both on the chemical reactivity of the surface site located below the tip and on the tip-sample distance. Metal dissolution from the anodic sites releases M^{z+} cations that are detected at the SECM tip through their conversion to another redox state. Thus, SECM has been successfully employed to monitor metastable pit formation on austenitic steel under open circuit conditions [10], as well as metal dissolution from either inclusions in alloys [11-13] or defects in polymer-coated materials [14-16]. On the other hand, in neutral or alkaline environments, dissolved oxygen in the electrolyte is consumed at the cathodic sites, thus local oxygen depletion at the cathodic sites can also be monitored at the SECM tip [17-20]. In the previous studies, noble metal microelectrodes were employed as tips for amperometric operation of the SECM, but the combination of SECM in potentiometric operation and antimony UME's makes possible pH imaging [21,22] for the characterization of a variety of systems, including corrosion reactions [23-26]. By using this experimental procedure, it has been recently shown that complex and highly localized chemical reactions occur during the first hour of immersion of zinc in substitute sea-water leading to heterogeneous pH distributions in excess of 3 pH units of sub-millimeter dimensions [3]. That is, metal hydrolysis and formation of various corrosion products are

already in operation at very early stages of zinc corrosion, and they are heterogeneously distributed over the metal surface.

Another powerful microelectrochemical technique is the scanning vibrating electrode technique (SVET), widely employed in the field of corrosion science in numerous applications: localized corrosion [27-30], galvanic corrosion [31,32], corrosion inhibitors [33-36], and microbiological corrosion [37], to name a few. This technique employs a vibrating reference microelectrode to detect the potential gradients produced in the proximity of a reacting surface, with respect to the value obtained in the bulk electrically-neutral solution, Electrical fields are produced by the diffusional flux of ionic species generated and/or consumed at the reacting surface, and they may eventually converted into ionic currents by taking in account the electrical conductivity of the electrolyte. in a solution, caused by a concentration gradient. SVET it is based on the detection of electric fields generated in the proximity of a reacting surface, with respect to the value obtained in the bulk electrically-neutral solution. Because of the tendency of zinc to undergo a non-general corrosion [18,38-40], ionic fluxes originated by the distribution of anodic and cathodic sites, on the metal surface at its initial stages, can be detected by SVET.

The aim of this work was to investigate the initial stages of zinc corrosion, immersed in substitute ocean water, and visualize at micrometric and sub-micrometric scales, the local formation of cathodic and anodic sites during this experiment.

2. EXPERIMENTAL

2.1. Material and sample preparation

Analytical grade zinc foil (99.99%), of thickness of 1.5 mm, was cut into square specimens of 5 mm × 5 mm dimensions. Additionally, a few samples were cut into 1 mm × 5 mm dimensions for SECM imaging as described in ref. [3]. Then, they were embedded in an epoxy resin sleeve (approximate diameter 3 cm) and mounted in so that only the square area formed the testing substrate. The front side of the mounts was ground to mirror surface with silicon carbide paper down to 4000 grit and subsequently polished using an ethanol and alumina suspension with 0.3 μm particle size, immediately before the experiments. The resulting surfaces were washed with 96%(v/v) ethanol in an ultrasonic bath, allowed to dry in air, and finally surrounded laterally by sellotape, thus creating a small container for the electrolyte solution.

Substitute ocean water (pH = 8.3) was prepared according to ASTM standard [41], with analytical grade reagents and Millipore twice-deionized water. The synthetic water was diluted in the ratio 1:1000 for testing (herein named substitute ocean water (diluted), pH = 6.2). The solution was naturally aerated and experiments were conducted at ambient temperature (18 °C). The metal sample was left unpolarized, thus effectively at its open circuit potential in the electrolyte. The electrochemical cell for SVET was completed using the corresponding microelectrodes for reference [18].

2.2. Instrumentation and experimental procedure

The scanning vibrating electrode instrumentation was manufactured by Applicable Electronics Inc. (Forestdale, MA, USA). A Micro Probe PI200101F microelectrode was used, consisting of Pt/Ir (80%/20%) wire, which was platinized in order to produce a spherical platinum black deposit of 20 μm diameter. The sample container was mounted horizontally facing upwards and as filled up with 5 mL of substitute ocean water (diluted). The experiments were carried out with the electrode tip vibrating in a plane perpendicular to the sample, at an amplitude of 20 μm and with frequency 235 Hz. Tip to substrate distance was fixed at 80 μm, and all measurements were done at the free corrosion potential. A platinum black wire was used as reference electrode, thus completing the electrochemical cell. The ionic current maps were obtained by scanning an area of 25 mm^2 approximately, forming a 50 × 50 points matrix in X-Y plane, making up a total of 2500 data points.

Local pH distributions were imaged using a scanning electrochemical microscope (SECM) supplied by Sensolytics (Bochum, Germany). The instrument was built around a PalmSens (Utrecht, The Netherlands) electrochemical interface, all controlled with a personal computer. Electrodes made of antimony and coated by its metal oxide have the ability to behave as a pH sensor [25]. The fabrication of the microelectrode is initiated by heating antimony powder in a melting pot with the help of a gas flame, then it is introduced in a Pyrex glass micropipette under suction. Antimony-filled micropipette is then pulled to produce a smaller size glass capillary, and then, it is introduced in the lumen of a second micropipette with the tip reaching out for about 15 mm. Finally, liquid mercury and a copper wire were then inserted into the lumen of the thicker capillary to provide electrical contact, using instant liquid adhesive to seal both ends. Antimony tips had a 40-μm-diameter active surface approximately. The pH calibration of the antimony microelectrodes was made using a sequence of eight buffer solutions covering the $4.0 \leq pH \leq 11.0$ range. The sample container was filled with 3.5 mL of substitute ocean water (non-modified), and the electrochemical cell was completed with an Ag/AgCl/(3 M) KCl electrode as reference. A video camera was used to further assist positioning of the tip close to the surface. A homemade voltage follower based on a 10^{12} Ω input impedance operational amplifier was connected between the electrochemical cell and the potentiometric input of the system [3,42]. Scan maps of pH changes were obtained, by scanning the tip parallel to the sample surface, at 30 μm constant height operation. SECM images were recorded scanning an area of 4000 μm × 1000 μm using a scan rate of 50 μm s^{-1}.

3. RESULTS AND DISCUSSION

It has been recently shown that Zn corrosion in substitute sea water (non-modified) leads to alkalization at the cathodic sites (equation (1)), whereas local acidification of the sea water down to 4.4 occurred at the anodic sites as a consequence of metal ion hydrolysis [3], according to equations (2) and (3):

$$O_2 + 2H_2O + 4e^- \rightarrow 4OH^- \tag{1}$$
$$Zn \rightarrow Zn^{2+} + 2e^- \tag{2}$$
$$Zn^{2+} + H_2O \rightarrow Zn(OH)^+ + H^+ \tag{3}$$

Therefore, when corrosion occurs, a release of Zn cations takes place at the anodic sites, and they can react with the solvent molecules to form zinc oxi-hydroxide anions [43] (equation (3)). As result, heterogeneous pH distributions were observed within 1 hour of exposure as shown in Figure 1 (i.e., at early stages of zinc corrosion). Observation of this pH map evidences that the anodic activity is highly localized at the upper left of the exposed sample of 1 mm × 5 mm dimension, whereas the rest of the surface behaves as a source of electrons for the electrochemical reduction of dissolved oxygen. Therefore, a progressive increase of the pH towards alkaline values is observed by moving away from the anodic region, both upwards and downwards in the image, though values are effectively more alkaline at the bottom due to the greater distances from the metal dissolution site available there. It was also observed that a complex variety of zinc corrosion products were formed at this early stages of exposure, consuming at least a fraction of the OH$^-$ ions, which are even observable with low-magnification optical microscopy imaging as shown in Figure 2. As result, partial or complete blocking of the initial anodic region has occurred already within 1 hour of exposure to substitute ocean water (non-modified), and it is hypothesized that the anodic region has necessarily migrated to another more exposed site on the metal surface. Unfortunately, the validity of this hypothesis could not be unambiguously established on the basis of either the pH map given in Figure 1 or the optical micrographs in Figure 2. Yet, a detailed observation of the pH map may be consistent with the local onset of anodic activity at the upper right side of the sample as evidenced by a local pH minimum. Furthermore, the pH values reached there (namely around 6.4) are too low for the precipitation of zinc oxi-hydroxides [1], thus indicating the physical separation of the precipitation front with respect to the actual anodic and cathodic sites [3], as it has been observed in the case of degradation reactions at electroplated, hot-dip galvanized cut edges and zinc foil on steel, exposed to model sodium chloride solutions [44-47]. In summary, complex and highly localized chemical reactions occur at the initiation of the corrosion of zinc in chloride environments.
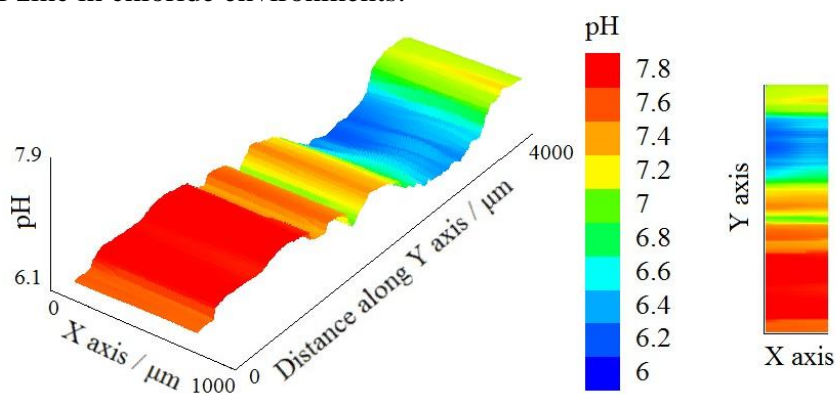

Figure 1. Distribution pH map recorded on the zinc surface after immersion in substitute ocean water (non-modified) during one hour. Adapted from ref. [3].
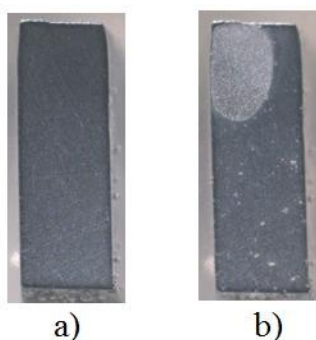
Figure 2. Optical micrographs of a zinc sample (a) before, and (b) after immersion in substitute ocean water (non-modified) during one hour for recording the pH distribution map by SECM given in Figure 1. The dimensions of the zinc plate are 1 mm × 5 mm.

In order to in situ monitor even earlier stages of zinc corrosion in substitute sea-water, a less aggressive situation was produced by 1:1000 dilution of the test environment (i.e., substitute ocean water (diluted)), and the time evolution of the system was followed with high spatial resolution by SVET. As it has been introduced above, a release of Zn cations takes place at the anodic sites according to equation (2). These metal cations generate positive current density values around the anodes, while the electrons flow to adjacent cathodic areas, leading to a flux of negative ionic current in the electrolyte, which in turn causes potential gradients to exist in the solution close to anodic sites of localized corrosion due to the formation of OH$^-$ anions according to equation (1). That is, an upward flow of OH$^-$ anions emerges from the surface cathodic regions, and these are detected by SVET as negative current densities.

The activation and subsequent corrosion of zinc in substitute ocean water (diluted) can be followed from the inspection of the SVET images shown in Figures 3-5, which correspond to the early stages of metal corrosion up to 5 hours from exposure. It can be observed the formation of both cathodic and anodic sites on the surface of the metal. As long as corrosion proceeds, due to the reactions (1) and (2), localized positive and negative ionic fluxes arise from the metal surface.
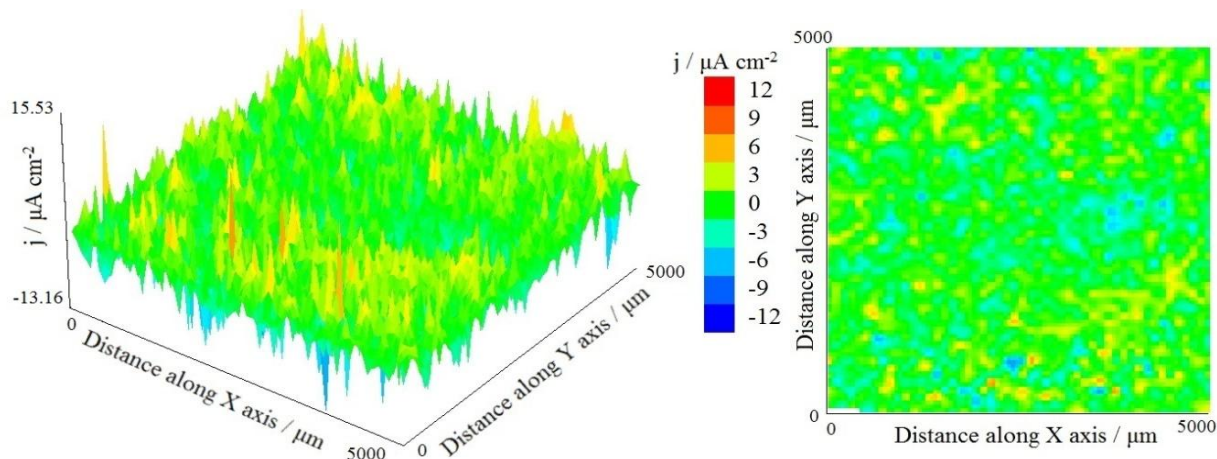

Figure 3. Current density map of a pure zinc sample after exposure to substitute ocean water (diluted) for 1 hour.
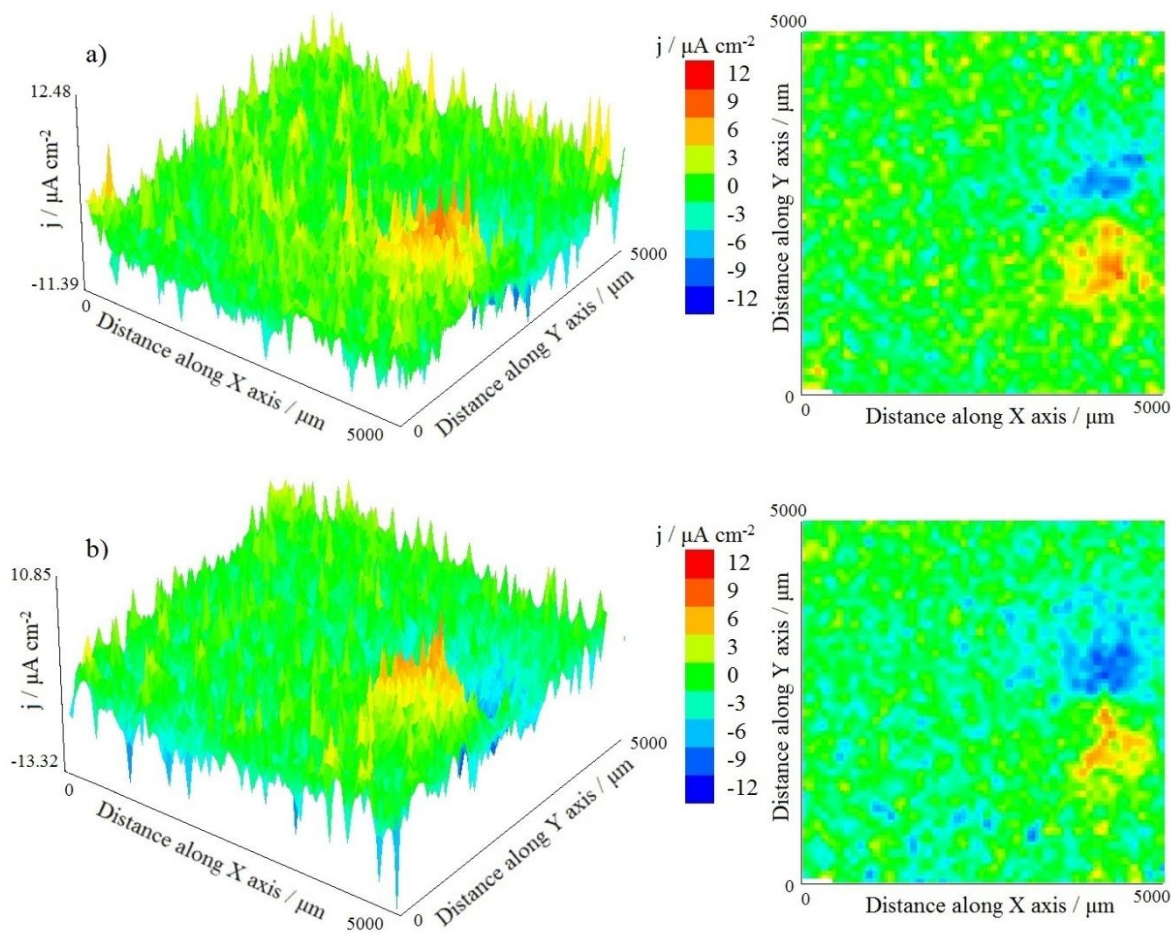
Figure 4.- Current density maps of a pure zinc sample after exposure to substitute ocean water (diluted) for: a) 2, and b) 3 h.

Though the SVET image recorded 1 hour immersion in the diluted substitute ocean water (Fig. 3) do not easily evidence the occurrence of distributed anodic and cathodic sites and the recorded signal may be regarded to arise from background noise, the early stages of metal activation can be already observed by comparison with the SVET maps recorded at longer exposures given in Figure 4. That is, a greatly localized anodic site, attributed to the nucleation of a corrosion pit on the metal surface, is observed at the right side in the lower half of the map recorded after 2 hours exposure, and continues being observable for the remaining of the experiment, though with varying magnitude (compare Figures 3 and 4). The correspondence of a localized anodic site and a major fraction of the cathodic activity in the adjacent metal surface clearly evidenced in the maps given in Figure 4, can also be correlated to the same locations of the Figure 3 that otherwise seemed featureless. Therefore, one can conclude that there is corrosion activity already at the first hour of immersion in the diluted substitute ocean water (i.e., Figure 3).
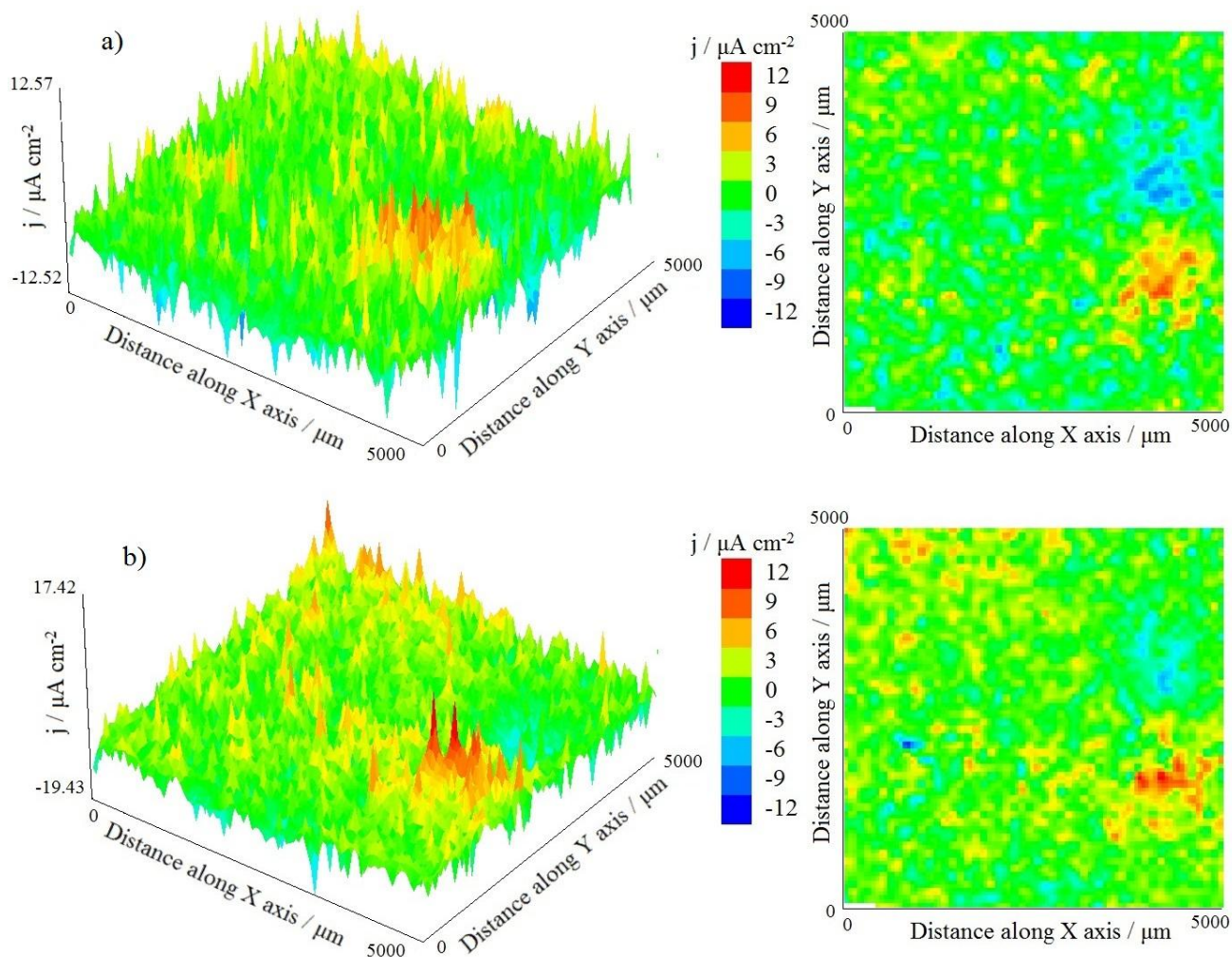
Figure 5.- Current density maps of a pure zinc sample after exposure to substitute ocean water (diluted) for: a) 4, and b) 5 h.

The propagation of the nucleated corrosion pit is evidenced by the greater positive current fluxes observed over the anodic site at 2 hours exposure, whereas the cathodic activity is more spread along the surface of the metal, reaching at further distances from the corroding site as time further elapses (compare the SVET maps recorded shown in Figure 4 a) and b), recorded after 2 and 3 hours exposure, respectively). The SVET maps indicated that metal dissolution from the nucleated pit at the right of the image was progressively diminishing in the following maps given in Figure 3, corresponding to longer exposures. In fact, this may indicate that precipitation of zinc oxi-hydroxides might have already occurred adjacent to the corroding pit, effectively leading to a partial blockage of the surface available for the charge transfer reactions. Yet, the images evidence the progressive activation of new anodic sites at the top left of the image, effectively leading to a shift of the anodic and cathodic sites on the surface with the progress of the corrosive attack, which eventually may lead, at sufficiently long exposures, to the observation that the whole surface of the metal is covered by corrosion products. The latter is a typical observation of retrieved samples taken from natural exposures in ocean water [3].

The SVET results are also consistent with the development of localized pH distributions on the metal surface, for local acidification should occur over the corroding single pits formed on zinc according to equations (2) and (3), whereas alkalization will occur on the remaining metal surface as result of oxygen reduction given by equation (1). Thus, the SVET results obtained in dilute substitute ocean water are in good agreement with the previous reports of highly localized metal dissolution (i.e., zinc runoff) and precipitation processes on zinc metal occur at the early stages of zinc corrosion in substitute ocean water as derived from SECM measurements (cf. Figure 1). Furthermore, both scanning microelectrochemical techniques supply valuable and complementary insights on the mechanism of corrosion processes, as illustrated herein by the corrosion of zinc in marine environments.

4. CONCLUSIONS

The localized distributions of anodic and cathodic activities on zinc metal/electrolyte interface, exposed to substitute ocean water (diluted), have been mapped in situ using SVET. The data provide in situ information on the local ionic fluxes produced in the electrolyte as result of the electrochemical corrosion reactions that occurred on the zinc surface, even in the first hours of the process. The maps demonstrated the evolution of the corrosion process, since the nucleation and propagation of corroding pits on the metal. Since the values and distribution of the anodic current densities will be influenced by the formation of insoluble corrosion products, zinc ions release and pH local changes, the time evolution of the maps allows to more adequately characterize the complex chemical process involved in zinc corrosion in sea-water with high spatial resolution. The use of SVET as microelectrochemical technique provides useful information for the characterization of the initial stages of zinc corrosion behavior in substitute ocean water.

References

1. S. Thomas, N. Birbilis, M.S. Venkatraman, I.S. Cole, *Corrosion,* 68 (2012) 015009.
2. S. Thomas, I.S. Cole, M. Sridhar, N. Birbilis, *Electrochim. Acta,* 97 (2013) 192.
3. E. Mena, L. Veleva, R.M. Souto, *Int. J. Electrochem. Sci.,* 10 (2015) 7596.
4. S. Thomas, I.S. Cole, N. Birbilis, *J. Electrochem. Soc.,* 160 (2013) C59.
5. R. Baboian (Ed.), *Electrochemical Techniques for Corrosion Engineering,* National Association of Corrosion Engineers, Houston, TX, (1987).

6.   P. Marcus, F. Mansfeld (Eds.), *Analytical Methods in Corrosion Science and Engineering*, CRC Press, Boca Raton, FL, (2005).

7.   R. Oltra, V. Maurice, R. Akid, P. Marcus (Eds.), *Local Probe Techniques for Corrosion Research*, Woodhead Publishing, Cambridge, (2007).

8.   R.M. Souto, S.V. Lamaka, S. González, in: A. Méndez-Vilas, J. Díaz (Eds.), *Microscopy: Science, Technology, Applications and Education*, Vol. 3, Formatex Research Center, Badajoz, Spain, (2010), p. 1769.

9.   M.B. Jensen, D.E. Tallman, in: A.J. Bard, C.G. Zoski (Eds.), *Electroanalytical Chemistry, A Series of Advances*, Vol. 24, CRC Press, Boca Raton, FL, (2012), p. 171.

10. Y. González-García, G.T. Burstein, S. González, R.M. Souto, *Electrochem. Commun.*, 6 (2004) 637.

11. C.H. Paik, H.S. White, R.C. Alkire, *J. Electrochem. Soc.,* 147 (2000) 4120.

12. C.H. Paik, R.C. Alkire, *J. Electrochem. Soc.,* 148 (2001) B276.

13. K. Fushimi, M. Seo, *Electrochim. Acta,* 47 (2001) 121.

14. R.M. Souto, Y. González-García, S. González, *Corros. Sci.,* 47 (2005) 3312.

15. A.M. Simões, D. Battocchi, D.E. Tallman, G.P. Bierwagen, *Corros. Sci.,* 49 (2007) 3838.

16. R.M. Souto, J.J. Santana, L. Fernández-Mérida, S. González, *Electrochim. Acta,* 56 (2011) 9596.

17. A.C. Bastos, A.M. Simões, S. González, Y. González-García, R.M. Souto, *Electrochem. Commun.,* 6 (2004) 1212.

18. A.M. Simões, A.C. Bastos, M.G. Ferreira, Y. González-García, S. González, R.M. Souto, *Corros. Sci.,* 49 (2007) 726.

19. R.M. Souto, L. Fernández-Mérida, S. González, *Electroanal.,* 21 (2009) 2640.

20. S. González, J.J. Santana, Y. González-García, L. Fernández-Mérida, R.M. Souto, *Corros. Sci.,* 53 (2011) 1910.

21. B.R. Horrocks, M.V. Mirkin, D.T. Pierce, A.J. Bard, G. Nagy, K. Toth, *Anal. Chem.*, 65 (1993) 1213.

22. M. Arca, A.J. Bard, B.R. Horrocks, T.C. Richards, D.A. Treichel, *Analyst,* 119 (1994) 719.

23. B. Kovács, B. Csóka, G. Nagy, R.E. Gyurcsányi, K. Toth, *Electroanal.,* 11 (1999) 349.

24. B. Csóka, B. Kovács, G. Nagy, *Biosens. Bioelectron.*, 18 (2003) 141.

25. J. Izquierdo, L. Nagy, Á. Varga, J.J. Santana, G. Nagy, R.M. Souto, *Electrochim. Acta,* 56 (2011) 8846.

26. J. Izquierdo, L. Nagy, I. Bitter, R.M. Souto, G. Nagy, *Electrochim. Acta,* 87 (2013) 283.

27. H.S. Isaacs, Y. Ishikawa, *J. Electrochem. Soc.,* 132 (1985) 1288.

28. V. Vignal, H. Krawiec, O. Heintz, R. Oltra, *Electrochim. Acta,* 52 (2007) 4994.

29. R. Zlatev, B. Valdez, M. Stoycheva, R. Ramos, S. Kiyota, *Int. J. Electrochem. Sci.,* 6 (2011) 2746.

30. J. Izquierdo, L. Martín-Ruíz, B.M. Fernández-Pérez, R. Rodríguez-Raposo, J.J. Santana, R.M. Souto, *J. Electroanal. Chem.*, 728 (2014) 148.

31. H.S. Isaacs, *Corros. Sci.,* 28 (1988) 547.

32. R.M. Souto, Y. González-García, A.C. Bastos, A.M. Simões, *Corros. Sci.,* 49 (2007) 4568.

33. S.M. Powell, H. McMurray, D. Worsley, *Corrosion*, 55 (1999) 1040.

34. S. Powell, *Surf. Eng.*, 16 (2000) 169.

35. S. Kallip, A.C. Bastos, M.L. Zheludkevich, M.G.S. Ferreira, *Corros. Sci.,* 52 (2010) 3146.

36. S. Kallip, A.C. Bastos, K.A. Yasakau, M.L. Zheludkevich, M.G.S. Ferreira, *Electrochem. Commun.,* 20 (2012) 101.

37. M.J. Franklin, D.C. White, H.S. Isaacs, *Corros. Sci.,* 32 (1991) 945.

38. I.S. Cole, W.D. Ganther, S.A. Furman, T.H. Muster, A.K. Neufeld, *Corros. Sci.,* 52 (2010) 848.

39. R.M. Souto, Y. González-García, D. Battistel, S. Daniele, *Chem. Eur. J.*, 18 (2012) 230.

40. M.A. Amin, S.S.A. El-Rehim, F.D.A.A. Reis, I.S. Cole, *Ionics,* 20 (2014) 127

41. D1141-98, *Standard Practice for the Preparation of Substitute Ocean Water*, ASTM International, West Conshohocken, PA, (2008).
42. B.M. Fernández-Pérez, J. Izquierdo, S. González. R.M. Souto, *J. Solid State Electrochem.,* 18 (2014) 2983.
43. S.V. Lamaka, R.M. Souto, M.G.S. Ferreira, in: A. Méndez-Vilas, J. Díaz (Eds.), *Microscopy: Science, Technology, Applications and Education*, Vol. 3, Formatex Research Center, Badajoz, Spain, (2010), p. 2162.
44. A.C. Bastos, A.M. Simões, M.G. Ferreira, *Port. Electrochim. Acta*, 21 (2003) 371.
45. A.M. Simões, J.C.S. Fernandes, *Prog. Org. Coat.,* 69 (2010) 219.
46. S.M. Manhabosco, R.J.C. Batista, S. Neves da Silva, L.F.P. Dick, *Electrochim. Acta,* 168 (2015) 89.
47. A.G. Marques, M.G. Taryba, A.S. Panão, S.V. Lamaka, A.M. Simões, *Corros. Sci.,* 104 (2016) 123.